Putative chanzyme activity of TRPM2 cation channel is unrelated to pore gating

Balázs Tóth[a,b], Iordan Iordanov[a,b], and László Csanády[a,b,1]

[a]Department of Medical Biochemistry and [b]Magyar Tudományos Akadémia - Semmelweis Egyetem Lendület (MTA-SE) Ion Channel Research Group, Semmelweis University, Budapest H-1094, Hungary

Edited by Christopher Miller, Howard Hughes Medical Institute, Brandeis University, Waltham, MA, and approved October 21, 2014 (received for review July 2, 2014)

Transient receptor potential melastatin 2 (TRPM2) is a Ca^{2+}-permeable cation channel expressed in immune cells of phagocytic lineage, pancreatic β cells, and brain neurons and is activated under oxidative stress. TRPM2 activity is required for immune cell activation and insulin secretion and is responsible for postischemic neuronal cell death. TRPM2 is opened by binding of ADP ribose (ADPR) to its C-terminal cytosolic nudix-type motif 9 (NUDT9)-homology (NUDT9-H) domain, which, when expressed in isolation, cleaves ADPR into AMP and ribose-5-phosphate. A suggested coupling of this enzymatic activity to channel gating implied a potentially irreversible gating cycle, which is a unique feature of a small group of channel enzymes known to date. The significance of such a coupling lies in the conceptually distinct pharmacologic strategies for modulating the open probability of channels obeying equilibrium versus nonequilibrium gating mechanisms. Here we examine the potential coupling of TRPM2 enzymatic activity to pore gating. Mutation of several residues proposed to enhance or eliminate NUDT9-H catalytic activity all failed to affect channel gating kinetics. An ADPR analog, α-β-methylene-ADPR (AMPCPR), was shown to be entirely resistant to hydrolysis by NUDT9, but nevertheless supported TRPM2 channel gating, albeit with reduced apparent affinity. The rate of channel deactivation was not slowed but, rather, accelerated in AMPCPR. These findings, as well as detailed analyses of steady-state gating kinetics of single channels recorded in the presence of a range of concentrations of ADPR or AMPCPR, identify TRPM2 as a simple ligand-gated channel that obeys an equilibrium gating mechanism uncoupled from its enzymatic activity.

nonequilibrium | channel enzyme | ADP ribose analog | Nudix motif | ligand-gated channel

Transient receptor potential melastatin 2 (TRPM2) belongs to the TRP protein family and is abundantly expressed in brain neurons, bone marrow, phagocytes, pancreatic β cells, and cardiomyocytes, where it forms Ca^{2+}-permeable nonselective cation channels that open under oxidative stress. On contact with pathogens, phagocytic cells produce reactive oxygen species (ROS); the resulting activation of TRPM2 provides the Ca^{2+} influx necessary for cell migration and chemokine production (1). In pancreatic β cells, TRPM2 activity contributes to glucose-evoked insulin secretion; TRPM2 knock-out mice show higher resting blood glucose levels and impaired glucose tolerance (2).

TRPM2 activity is also linked to several pathologic conditions that lead to apoptosis (3). Reperfusion after ischemia results in ROS generation; consequent Ca^{2+} influx through TRPM2 causes Ca^{2+} dysregulation and cell death. Certain neurodegenerative diseases, such as Alzheimer's disease, also involve oxidative stress and TRPM2 activation. In contrast, a loss-of-function TRPM2 mutation identified in patients with amyotrophic lateral sclerosis and Parkinson's disease dementia (4), as well as two TRPM2 mutations associated with bipolar disorder (5), suggest loss of TRPM2 activity can also cause disease.

Similar to most TRP family ion channels, the TRPM2 channel is a homotetramer, and its transmembrane (TM) architecture resembles that of voltage-gated cation channels (6, 7). In addition to the TM domain and an N-terminal cytosolic domain of unknown function, TRPM2 contains an ∼270-residue C-terminal cytosolic nudix-type motif 9 (NUDT9)-homology (NUDT9-H) domain. The latter shows high (∼50%) sequence homology to the soluble mitochondrial enzyme NUDT9, an active ADP ribose (ADPR) pyrophosphatase (ADPRase) from the Nudix hydrolase family, which splits ADPR into AMP and ribose-5-phosphate (8). TRPM2 channels are coactivated by ADPR binding to NUDT9-H (9) and by Ca^{2+} binding to unidentified intracellular binding sites (10). ADPR is the key that links TRPM2 activation to oxidative stress; in living cells exposed to ROS, ADPR is released from mitochondria (9). In the past, studying TRPM2 channel gating at steady state has been limited by rapid deactivation of TRPM2 currents in cell-free patches (10). This rundown was recently shown to involve a conformational change of the ion selectivity filter, which could be completely prevented by a pore-loop substitution. This "T5L" TRPM2 variant, which shows no rundown but preserves intact regulation of gating by Ca^{2+} and ADPR (11), provides an unprecedented opportunity to study TRPM2 gating at steady state.

Early studies reported slow (∼0.1 s^{-1}) but detectable ADPRase activity of isolated purified NUDT9-H (8, 12), classifying TRPM2 into the special group of channel-enzymes ("chanzymes") that includes TRPM6 and TRPM7 (3) and the CFTR cystic fibrosis transmembrane conductance regulator (CFTR) chloride ion channel (13). TRPM2 pore opening/closure happens on the timescale of the reported ADPRase activity (11), which is consistent with coupling between gating and catalytic activity, as demonstrated for CFTR in which pore gating follows an irreversible cycle tightly

Significance

Ion channels are protein pores that allow passive transmembrane ion flow. These pores are opened and closed (gated) by various cellular signals. Typically, the mechanism of gating conformational changes is an equilibrium process, but for some channels, gating is an irreversible cycle, for example, linked to an enzymatic activity. For equilibrium mechanisms, channel activity is readily modulated by energetic stabilization of closed or open states, whereas for cyclic gating, alteration of transition-state stabilities most effectively modulates activity. Transient receptor potential melastatin 2 (TRPM2), a cation channel involved in multiple physiologic and pathophysiologic processes, possesses enzymatic activity, which cleaves its activating ligand. This work addresses, and rules out, a suggested link between that catalysis and pore gating in TRPM2, classifying it among the channels that gate at equilibrium.

Author contributions: B.T., I.I., and L.C. designed research; B.T., I.I., and L.C. performed research; L.C. contributed new reagents/analytic tools; B.T., I.I., and L.C. analyzed data; and L.C. wrote the paper.

The authors declare no conflict of interest.

This article is a PNAS Direct Submission.

Freely available online through the PNAS open access option.

[1]To whom correspondence should be addressed. Email: csanady.laszlo@med.semmelweis-univ.hu.

This article contains supporting information online at www.pnas.org/lookup/suppl/doi:10.1073/pnas.1412449111/-/DCSupplemental.

linked to ATP binding and hydrolysis at conserved cytosolic domains (14).

The involvement of TRPM2 in multiple diseases has made it an emerging therapeutic target. Depending on the disease, both inhibition (e.g., stroke, myocardial infarction, Alzheimer's disease, chronic inflammation, hyperinsulinism) and stimulation (e.g., diabetes, amyotrophic lateral sclerosis, Parkinson's disease dementia, bipolar disorder) of TRPM2 activity might be useful therapeutically. Because TRP family channels are involved in diverse processes (3), any useful TRPM2 agonists/antagonists will need to be highly selective. This singles out the NUDT9-H domain, the component unique to TRPM2, as the most attractive drug target. The significance of understanding whether ADPRase activity and gating are coupled is that optimal strategies for modulating fractional occupancy of a particular conformational state are profoundly different for equilibrium systems than for nonequilibrium systems. For most ion channels, pore gating is an equilibrium process, and open probability is modulated simply by energetic stabilization of either open (activators) or closed (inhibitors) channel ground states. In contrast, channels that gate by a nonequilibrium cycle are most efficiently accumulated in either open or closed states by manipulating the stability of transition states for rate-limiting irreversible steps (15). The aim of this study was to examine the tightness of coupling between the ADPRase cycle and specific gating transitions in TRPM2.

Results

Mutations of Residues Key for Catalysis in Nudix Family Enzymes Have Little Effect on TRPM2 Channel Gating. In inside-out patches, in the presence of saturating (125 μM) intracellular Ca^{2+}, wild-type (WT) TRPM2 currents are activated by cytosolic ADPR with an apparent affinity of ∼1 μM (Fig. 1 *A* and *G*; cf. refs. 10, 16) and deactivate slowly, with a time constant of ∼2 s, on rapid removal of ADPR (Fig. 1*A*, green fit line, and Fig. 1*K*; cf. ref. 11). Fractional activity in 1 μM ADPR reports ADPR binding affinity, whereas the slow current decay rate (∼0.5 s^{-1}) on ADPR removal is on the order of the ADPRase turnover rate reported (12) for the purified NUDT9-H domain (∼0.1 s^{-1}), supporting a suggested (8) link between the enzymatic cycle and gating. The time constant of this current decay reflects the lifetime of an "active conformation" of the NUDT9-H domain; exit from this "active state" might correspond to dissociation of intact ADPR, ADPR hydrolysis, or perhaps dissociation of the hydrolysis products. We therefore tested how these macroscopic gating parameters are affected by catalytic site mutations.

All Nudix family enzymes contain the conserved Nudix box sequence motif $GX_5EX_7REX_2EE$, which forms a loop–helix structure essential for correct positioning of the substrate's pyrophosphate moiety and catalytic Mg^{2+} ions (17) (Fig. S1). Divergence of the terminal six residues of this motif between NUDT9 and NUDT9-H (R_{229}EFGEE$_{234}$ in NUDT9, but R_{1404}ILRQE$_{1409}$ in NUDT9-H; Fig. 1*B*) was found responsible (12, 17) for the ∼100-fold lower catalytic activity of the latter enzyme. Notably, in a crystal structure of NUDT9, the side chain of residue E230 coordinates the Mg^{2+} ion (17) (Fig. S1). The REF→RIL substitution reduced NUDT9 enzymatic activity by 100-fold (12, 17), and substitution EE→KK of the terminal two Nudix-box residues completely abolished it (12). By analogy, the QE→KK substitution of the terminal two Nudix-box residues in single-mutant Q1408K and E1409K and double-mutant Q1408K/E1409K TRPM2 channels may be expected to abolish ADPRase activity of NUDT9-H. However, neither substitution slowed channel deactivation (Fig. 1 *D–F* and *K*), and only the double-mutation Q1408K/E1409K modestly decreased the apparent affinity for current activation by ADPR (Fig. 1 *F* and *G*). Conversely, in an attempt to enhance the slow ADPRase activity of NUDT9-H, we regenerated the canonical REF motif in TRPM2 by introducing mutations I1405E, L1406F, and I1405E/L1406F. Both single mutants and the double mutant generated macroscopic ADPR-induced currents (Fig. 1 *H–J*), and none of these substitutions affected fractional activation by 1 μM ADPR (Fig. 1*G*) or deactivation rate after ADPR removal (Fig. 1*K*). Note that deactivation should have been accelerated if these

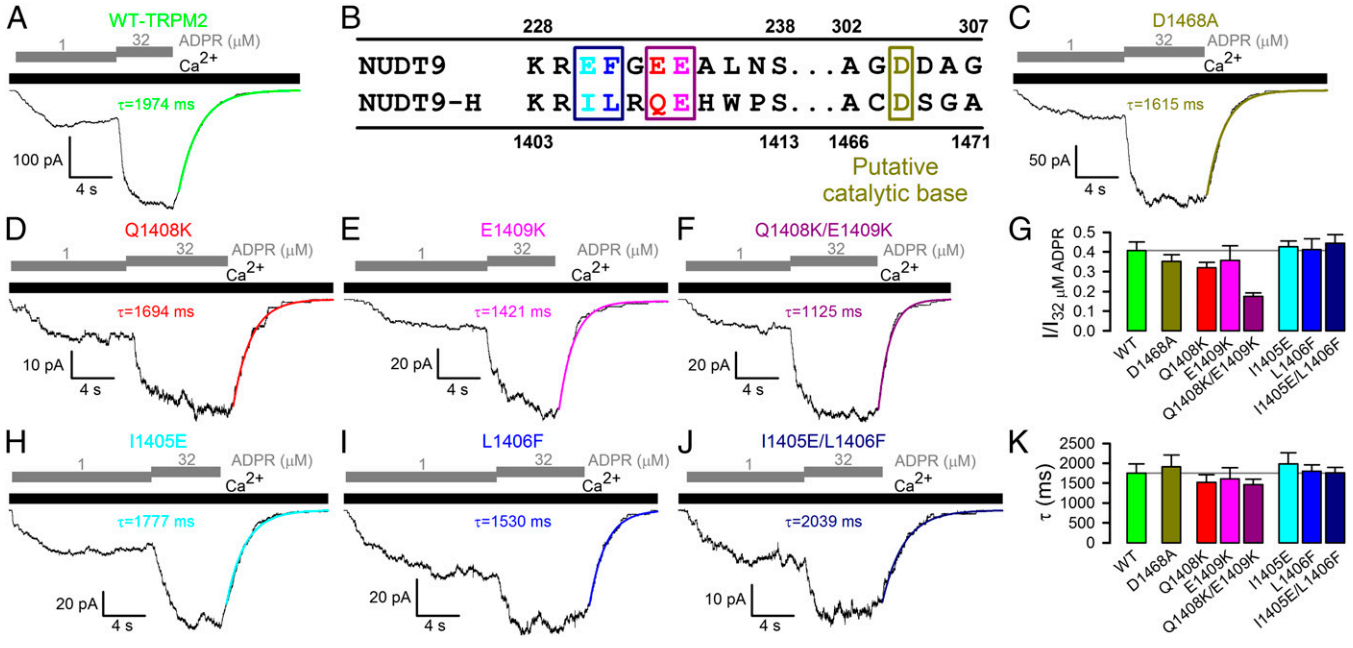

Fig. 1. Mutations of residues proposed to be key for catalysis have little effect on TRPM2 channel gating. (*A*, *C*, *D–F*, *H–J*) Inward macroscopic currents elicited by application of 125 μM Ca^{2+} (black bars) plus 1 or 32 μM ADPR (gray staggered bars) to the cytosolic faces of inside-out patches excised from *Xenopus* oocytes expressing human (*A*) WT, (*C*) D1468A, (*D*) Q1408K, (*E*) E1409K, (*F*) Q1408K/E1409K, (*H*) I1405E, (*I*) L1406F, and (*J*) I1405E/L1406F TRPM2 channels. Colored lines, single exponential fits to current relaxation time courses; τ, time constants. (*B*) Sequence alignment of NUDT9 and NUDT9-H Nudix boxes highlighting residues functionally important in NUDT9. (*G*) Fractional current activation (mean ± SEM) by 1 μM ADPR for WT and mutant TRPM2; steady current in 1 μM ADPR was normalized to that in 32 μM ADPR in the same patch. (*K*) Deactivation time constants (mean ± SEM) after ADPR removal, from single-exponential fits.

mutations accelerated ADPR hydrolysis and the latter rate limited channel closure.

Finally, D1468 of TRPM2 aligns with the catalytic base of *Escherichia coli* ADPRase. Although mutation of the diacidic motif at the analogous position of NUDT9 (D304/D305; Fig. 1*B*) reduced its ADPRase activity by ~15-fold (17), D1468A TRPM2 channels expressed well (Fig. 1*C*) and yielded channels with gating parameters indistinguishable from WT (Fig. 1 *G* and *K*).

TRPM2 Channel Activation Is Not Linked to Ligand Hydrolysis. Our mutational results suggested that ADPR hydrolysis might not be linked to channel gating. However, the catalytic mechanisms of Nudix enzymes are known to have diverged (17), leaving room for the alternative possibility that other residues are responsible for catalysis in NUDT9-H. As a complementary approach, therefore, we tested whether a nonhydrolyzable ADPR analog, α-β-methylene-ADPR (AMPCPR; ref. 18; Fig. 2*B*; the oxygen bridging the α and β phosphates is replaced by a methylene group), would support channel gating. We used the soluble and highly active NUDT9 protein (Fig. S2*B*) to verify resistance of AMPCPR to hydrolysis. Indeed, incubation of NUDT9 with AMPCPR did not result in the appearance of breakdown products, whereas ADPR was stoichiometrically converted into AMP and ribose-5-phosphate (Fig. 2*A*). In inside-out patches, cytosolic application of AMPCPR activated TRPM2 currents in a dose-dependent manner (Fig. 3*B*; in these and all subsequent experiments, we used the noninactivating T5L pore mutant, which allowed for longer experiments and, thus, repeated application of various tested nucleotides). However, the apparent affinity for current activation was ~40-fold lower relative to ADPR (Fig. 3*A*), and currents elicited by a quasi-saturating concentration of 400 μM AMPCPR remained only ~50% of those activated by a saturating concentration (32 μM) of ADPR (Fig. 3*C*, red versus blue symbols and fit lines). Thus, AMPCPR is a low-affinity partial agonist of TRPM2. The fact that a nonhydrolyzable analog readily opens TRPM2 channels clearly demonstrates that ligand hydrolysis is not required for TRPM2 channel opening.

TRPM2 Channel Deactivation Is Not Linked to Ligand Hydrolysis. To probe any potential requirement for ligand hydrolysis in TRPM2 channel deactivation, we tested whether macroscopic deactivation rate on sudden nucleotide removal is slowed for the nonhydrolyzable analog. On the contrary, deactivation after AMPCPR removal was accelerated ~threefold relative to that on removal of ADPR (Fig. 4), suggesting that the lifetime of the activated state is not terminated by ligand hydrolysis. Of note, CFTR channels, in which pore closure is coupled to hydrolysis of the native ligand ATP (19), nevertheless close promptly when opened by the nonhydrolyzable analog adenylyl imidodiphosphate (AMPPNP), but

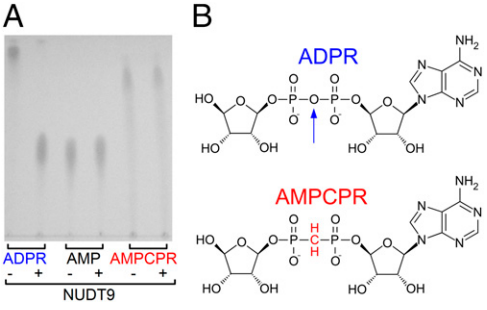

Fig. 2. AMPCPR is resistant to hydrolysis. (*A*) TLC analysis of ADPR, AMP, and AMPCPR samples before (–) and after (+) incubation with purified NUDT9 (see *SI Materials and Methods*). ADPR is degraded into AMP and ribose-5-phosphate; the latter is not visible on the TLC. (*B*) Structures of ADPR and AMPCPR. Vertical arrow highlights the oxygen bridge in ADPR that is cleaved by NUDT9.

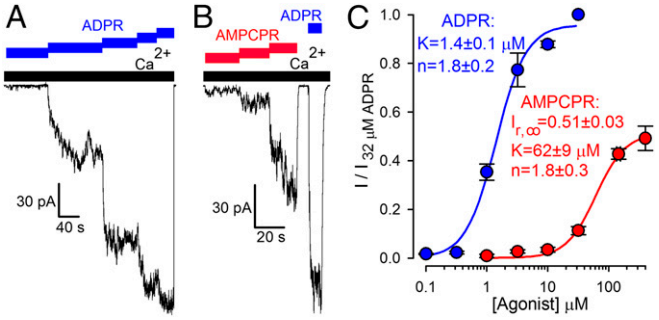

Fig. 3. Nonhydrolyzable ADPR analog is a low-affinity partial TRPM2 channel agonist. (*A* and *B*) T5L-TRPM2 currents are stimulated in a dose-dependent manner by cytosolic application of either (*A*) 0.32, 1, 3.2, 10, and 32 μM ADPR (blue staggered bar) or (*B*) 10, 32, and 200 μM AMPCPR (red staggered bar) in the presence of saturating cytosolic Ca^{2+} (black bars). Currents elicited in the same patches by saturating (32 μM) ADPR (blue bars) were used for normalization. (*C*) Normalized dose–response curves (mean ± SEM) for stimulation of macroscopic T5L-TRPM2 current by ADPR (blue symbols; replotted from ref. 11) and AMPCPR (red symbols). Solid lines are fits to the Hill equation.

they are arrested in the open state on binding of one ATP and one AMPPNP in ATP/AMPPNP mixtures (19). However, TRPM2 channels opened by ADPR/AMPCPR mixtures deactivated at rates intermediate between those measured for the two nucleotides, and no "locked-open" channels could be detected even under such conditions (Fig. S3), further supporting the conclusion that ligand hydrolysis is not required for TRPM2 channel closure.

Bursting Pattern of Single-Channel Activity in Saturating ADPR Suggests Two Types of Gate Closures. To better understand the mechanism by which ADPR gates TRPM2 channels, we studied the pattern of steady-state single-channel gating at low (1 μM) and high (32 μM) concentrations of ADPR (Fig. 5 *A* and *B*). Although the distributions of open dwell times (Fig. 5 *C* and *D*, *Right*) were reasonably fit by single exponentials (red lines), fitting the closed-time distributions required at least two exponential components (Fig. 5 *C* and *D*, *Left*, red fit lines), suggesting the presence of at least two types of closed states. [A simple C↔O model (Fig. 5*E*, blue dashed box) was inadequate to describe either data set (Fig. 5 *C* and *D*, blue dashed fit lines) and could be excluded with strong confidence at both concentrations of ADPR ($P = 2 \times 10^{-25}$ and 2×10^{-45}, respectively).] The result is a bursting gating pattern, with bursts of openings interrupted by brief ("flickery") closures and flanked by longer ("interburst") closures (Fig. 5 *A* and *B*; cf. ref. 10). In saturating ADPR, the mean duration of interburst closures was shortened but remained distinctly longer than that of flickery closures. Thus, entering a burst is not caused by ligand binding itself but, instead, reflects a conformational change after ligand binding, which becomes rate-limiting at high ADPR concentrations. To model gating of fully liganded TRPM2, we chose the three-state scheme $C_s^* \leftrightarrow O^* \leftrightarrow C_f^*$ (Fig. 5*E*, red box; C_s^*, O^*, and C_f^* are fully liganded closed-interburst, open, and flickery closed states, respectively; see *Discussion* for further support of this choice).

Reduced Stability of the Bursting State Explains Reduced Efficacy for Channel Activation by AMPCPR. Although, because of the slow gating rates, only a few transitions could be collected from any single channel recording (Fig. 5), patches with multiple channels provided sufficient gating events (Fig. S4) to reliably extract (see Materials and Methods) single-channel open probabilities (P_o; Fig. 6*A*) and mean open burst (τ_b; Fig. 6*B*) and interburst (τ_{ib}; Fig. 6*C*) durations over a range of concentrations of activating nucleotide, using either ADPR (blue) or AMPCPR (red) as the ligand. The reduced apparent affinity of AMPCPR for stimulating P_o (Fig. 6*A*, red versus blue symbols and fit lines), which

PHYSIOLOGY

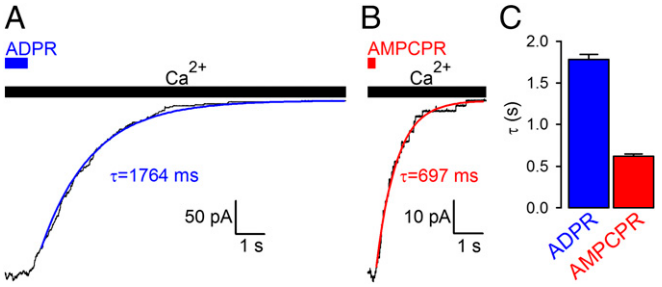

Fig. 4. Nonhydrolyzable ligand does not slow TRPM2 channel deactivation. (*A* and *B*) Decay time courses on nucleotide removal of macroscopic T5L-TRPM2 currents activated by quasi-saturating concentrations of (*A*) ADPR or (*B*) AMPCPR in the presence of saturating Ca^{2+}. Colored lines, single-exponential fits; τ, time constants. (*C*) Mean ± SEM deactivation time constants of T5L-TRPM2 channels opened by ADPR and AMPCPR.

replicated the observations on macroscopic currents (Fig. 3*C*), was caused by a reduced apparent affinity for shortening τ_{ib} (Fig. 6*C*), whereas τ_b (Fig. 6*B*) showed little dependence on agonist concentration. This suggests a reduced affinity of AMPCPR for binding to closed channels (Figs. 5*E* and 6*G*; step $C_s \leftrightarrow C_s^*$). In contrast, the reduced efficacy of AMPCPR originated from a distinct kinetic effect: Whereas at saturating AMPCPR, τ_{ib} asymptotically approached that measured in saturating ADPR (~1 s; Fig. 6*C*, red versus blue fit lines), τ_b remained ~threefold shorter (~1.5 s in AMPCPR versus ~5 s in ADPR; Fig. 6*B*, red versus blue symbols). In the framework of the $C_s^* \leftrightarrow O^* \leftrightarrow C_f^*$ gating scheme, these findings are explained by alteration (relative to ADPR) of a single rate, a ~threefold acceleration of rate $O^* \rightarrow C_s^*$ with AMPCPR (to ~0.7 s^{-1}; Fig. 6*G*). Furthermore, this scheme also predicts several effects on intraburst behavior for AMPCPR: acceleration of $rate_{O^* \rightarrow Cs^*}$ should entail a shortened mean open time $[\tau_o = (rate_{O^* \rightarrow Cs^*} + rate_{O^* \rightarrow Cf^*})^{-1}]$ and a reduced average number of flickery closures per burst ($n_f = rate_{O^* \rightarrow Cf^*}/rate_{O^* \rightarrow Cs^*}$), but unaltered mean flickery closed time duration $[\tau_f = (rate_{Cf^* \rightarrow O^*})^{-1}]$, all of which are readily observable in the data (Fig. 6 *D*, *F*, and *E*, respectively; red versus blue symbols).

What is the nature of the $C_s^* \rightarrow O^*$ conformational transition that initiates a channel open burst? Activating ligands stabilize the open state because they bind more tightly when the pore is open. In extreme cases, such as for the CFTR channel, the agonist is fully occluded and cannot be washed off while the channel is open. As a consequence, the mean open (burst) duration is insensitive to agonist concentration (19) and is identical to the time constant of macroscopic current deactivation after ligand removal (14). For TRPM2, τ_b and τ_o also do not depend strongly on [ADPR], but a slight trend for shorter τ_b and τ_o at very low, submicromolar nucleotide concentrations (Fig. 6 *B* and *D*, blue and red symbols) suggests that ADPR might not be completely occluded but remains somewhat exchangeable, even in open channels (Fig. 6*G*, semitransparent states O and C_f), although the open-state affinity for ADPR is much higher, as for a conventional ligand-gated channel. Indeed, macroscopic deactivation time constants (Fig. 4 and Fig. S5*A*) and mean open times measured during the deactivation time course (Fig. S4*B*) extend the plots in Fig. 6 *B* and *D* and reflect τ_b and τ_o at zero agonist concentration (Fig. S5 *C* and *D*).

Discussion

Ion channels are passive devices: When open, they allow diffusion of ions down their electrochemical gradient, a process that does not require energy input. For most ion channels, the gating conformational changes that open and close the pore are at thermal equilibrium and are not coupled to irreversible enzymatic reactions. Few exceptions to this rule exist. The only ion channel for which gating has been shown to be linked to an irreversible ATP hydrolysis cycle is the CFTR chloride ion channel, which belongs to the family of ATP Binding Cassette transporters and likely inherited this trait from an ancestral active pump (14). TRPM6 and TRPM7 contain an active kinase domain at their C termini, but the link between kinase activity and channel gating is unclear (20). The discovery of the ADPRase activity of the TRPM2 NUDT9-H domain (8) placed TRPM2 into the small group of chanzymes, raising the intriguing possibility that its gating might also be linked to an irreversible enzymatic cycle.

Parallel biochemical studies on NUDT9 and on the isolated NUDT9-H domain highlighted residues of importance for catalysis. The two orders of magnitude difference between catalytic rates of NUDT9 (~10 s^{-1}) and NUDT9-H (~0.1 s^{-1}) were explained by divergent sequences in the conserved Nudix motif (Fig. 1*B* and Fig. S1). Converting this motif in NUDT9 to a NUDT9-H-like sequence (REF→RIL substitution) indeed lowered NUDT9 catalytic turnover rate by ~100-fold (12). In addition, the reverse RIL→REF substitution in full-length TRPM2 abolished ADPR-induced whole-cell currents (21), which was interpreted to reflect acceleration of ADPR hydrolysis and, hence, limited residence time of the nucleotide on NUDT9-H. Although a double lysine substitution for the terminal two Nudix box residues that eliminated ADPRase activity of NUDT9 (12) did not abolish whole-cell channel currents when introduced into full-length TRPM2 (9), potential dramatic alterations in gating kinetics were not assessed, leaving room for a possible coupling between catalysis and gating. Indeed, for CFTR chloride channels in which pore closure is coupled to ATP hydrolysis, certain mutations that impair catalysis slow closure by ~100-fold, but do not reduce open probability (13, 19). In our experiments, RIL→REF substituted channels supported large ADPR-evoked currents with gating parameters indistinguishable from WT (Fig. 1 *H–J*). We attribute the lack of activity in the earlier study (21) to misfolding/misprocessing of the mutant protein in mammalian cells at 37 °C, but not in *Xenopus* oocytes incubated at 18 °C. We found the double lysine substitution Q1408K/E1409K to also allow robust functional surface expression (Fig. 1*F*; cf. ref. 9) and, with the exception of a slightly reduced apparent affinity for

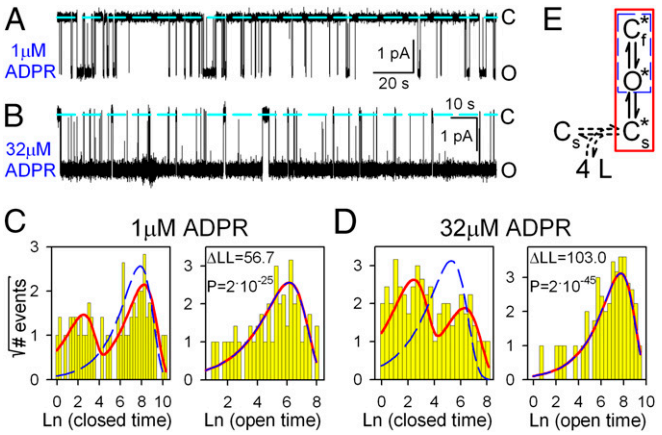

Fig. 5. Bursting gating pattern of single T5L-TRPM2 channels is evident even in saturating ADPR. (*A* and *B*) Current recordings from single T5L-TRPM2 channels in 125 μM cytosolic Ca^{2+} and (*A*) 1 or (*B*) 32 μM ADPR. Dashed lines, zero-current level. (*C* and *D*) Histograms (22) of closed (*Left*) and open (*Right*) dwell times of single channels gating in (*C*) 1 or (*D*) 32 μM ADPR, from the recordings in *A* and *B*, respectively. Dashed blue and solid red lines are maximum-likelihood fits to the dwell-time distributions by subsets of the scheme in *E*, framed in respective colors. Log-likelihood ratios (*ΔLL*) allow rejection of the C↔O model with significance *P* (29); similar *ΔLL* values (31.5–310.1) were obtained in six further single-channel patches. (*E*) Simplest gating scheme compatible with the dwell-time distributions. Boxed subsets generate identically colored fits in *C* and *D*. Asterisks mark fully liganded states. C_s^*, long (slow) closed state; O*, open state; C_f^*, brief (flickery) closed state. Horizontal dashed double arrow connects unliganded (C_s) and fully liganded (C_s^*) long closed states and represents sequential binding of four ligands.

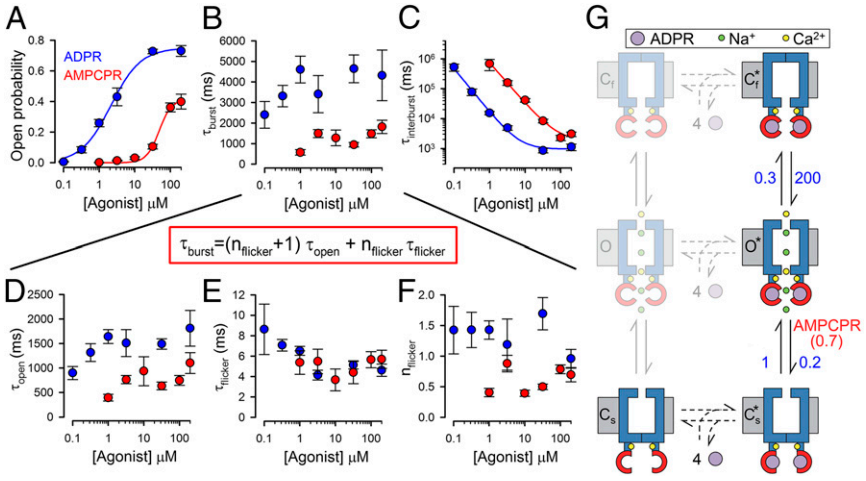

Fig. 6. Detailed kinetic analysis reveals molecular mechanism of nucleotide-dependent channel activation. (*A–F*) Dose–response curves (mean ± SEM) of (*A*) P_o, (*B*) τ_b, (*C*) τ_{ib}, (*D*) τ_o, (*E*) τ_f, and (*F*) n_f, for T5L-TRPM2 channels gating at steady state in 125 μM Ca^{2+} plus various concentrations of ADPR or AMPCPR (blue and red symbols, respectively), extracted by maximum-likelihood fitting of 199 well-resolved multichannel recordings from 124 patches (see *Materials and Methods* and Fig. S4). Note that τ_b is a function of the intraburst parameters in *D–F* (equation in red box). Solid lines in *A* are fits to the Hill equation [$P_o = P_{o;\infty}\cdot([L]^n/([L]^n+K^n)$]; those in *C* are fits to the inverse of the Hill equation [$\tau_{ib} = ([L]^n+K^n)/([L]^n\cdot\tau_{ib;\infty})$]. Fit parameters were (*A*) $P_{o;\infty} = 0.75 \pm 0.03$, $K = 2.1 \pm 0.3$ μM, $n = 1.0 \pm 0.1$ for ADPR and $P_{o;\infty} = 0.41 \pm 0.02$, $K = 48 \pm 6$ μM, $n = 2.5 \pm 0.5$ for AMPCPR; (*C*) $\tau_{ib;\infty} = 1.0 \pm 0.2$ s, $K = 7.1 \pm 1.9$ μM, $n = 1.5 \pm 0.1$ for ADPR and $\tau_{ib;\infty} = 1.8 \pm 0.8$ s, $K = 83 \pm 45$ μM, $n = 1.4 \pm 0.1$ for AMPCPR. (*G*) Cartoon, molecular interpretation of nucleotide-dependent TRPM2 gating. Numbers on vertical transitions are rates (s^{-1}). Blue, TM domain; upper constriction, selectivity filter; lower constriction, TM6 bundle crossing; red, NUDT9H domains; purple, activating nucleotides; yellow, Ca^{2+}; green, Na^+. Incomplete occlusion of the nucleotide might allow for ligand release in the bursting state (to putative states depicted in faint print).

ADPR (Fig. 1*G*), gating of this double mutant again remained similar to WT. Finally, we tested the role of residue D1468, which aligns with the catalytic base of the *E. coli* ADPRase (17), but D1468A TRPM2 gating also remained indistinguishable from WT (Fig. 1 *C*, *G*, and *K*).

As an alternative approach for probing the role of ADPR hydrolysis, we used the nonhydrolyzable analog AMPCPR (ref. 18; Fig. 2*B*), which we confirmed to be indeed completely resistant to hydrolysis, even by NUDT9 (Fig. 2*A*), an ADPRase ~100-fold more active than NUDT9-H (Fig. 2*A*). The nonhydrolyzable analog readily opened TRPM2 channels (Fig. 3*B*), albeit with reduced apparent affinity (Fig. 3*C*), and did not arrest the channels in the active (bursting) state, as indicated by an even accelerated deactivation rate on its removal (Fig. 4 *B* and *C*, red bar). In principle, the ADPR-induced active state might be more stable and require ligand hydrolysis for its prompt disassembly, whereas the AMPCPR-induced bursting state might be less stable and disassemble promptly, even without ligand hydrolysis. If that were the case, and hydrolysis of the four bound ADPR molecules was a concerted process [note that independent sequential hydrolysis would be expected to cause a sigmoidal deactivation time course, unlike the exponential relaxations observed here (e.g., Fig. 4*A*)], then binding of AMPCPR in only one subunit might be sufficient to prevent hydrolysis of ADPR in the other three, whereas bursting-state stability would be still dominated by the three native high-affinity ligands, causing prolonged arrest in the bursting state (cf. ref. 19). However, no such population of locked-open channels was detected in ADPR/AMPCPR mixtures (Fig. S3*A*); the observed intermediate deactivation rate (Fig. S3*B*) suggests simple energetically additive effects of all four bound nucleotides on bursting-state stability. Together, these results firmly establish that neither activation (entering a burst) nor deactivation (exiting a burst) of TRPM2 is linked to ligand hydrolysis: TRPM2 is a conventional ligand-gated channel, and its gating conformational changes are at thermodynamic equilibrium.

At least one open and two closed states could be resolved in single-channel dwell-time histograms, even at saturating ADPR (Fig. 5*D*), requiring a three-state scheme as a minimal gating model for fully liganded channels. Such a bursting gating pattern is equally well explained by a $C_s^*\leftrightarrow C_f^*\leftrightarrow O^*$ (CCO) or a $C_s^*\leftrightarrow O^*\leftrightarrow C_f^*$ (COC) scheme (22), but two arguments favor the COC choice here (Fig. 5*E*). First, whereas the COC scheme implies distinct slow and fast channel gates, the CCO scheme assumes a single gate, the opening of which is modeled by the $C_f^*\rightarrow O^*$ step. Therefore, for channels obeying the latter mechanism, partial agonists that are inefficient in opening the channel often prolong the mean dwell time in the C_f^* state (e.g., ref. 23); that is, the mean flickery closed time duration (τ_f). In contrast, for TRPM2, τ_f was unaltered in the presence of the partial agonist AMPCPR (Fig. 6*E*), suggesting the presence of two distinct gates: a slow gate regulated by nucleotide binding and an independent fast gate. Second, the COC scheme is also supported by the argument of parsimony: Using this scheme, the complex effects of AMPCPR on burst length (shortened τ_b; Fig. 6*B*) and intraburst kinetic parameters [shortened τ_o (Fig. 6*D*), unchanged τ_f (Fig. 6*E*), and reduced n_f (Fig. 6*F*)] are all explained by alteration of a single rate (acceleration of $rate_{O^*\rightarrow Cs^*}$; Fig. 6*G*), whereas the CCO scheme would require simultaneous alterations in three rates (increased $rate_{Cf^*\rightarrow Cs^*}$, slowed $rate_{Cf^*\rightarrow O^*}$, increased $rate_{O^*\rightarrow Cf^*}$) to achieve this result. Thus, the reduced (relative to ADPR) efficacy of AMPCPR is caused by less-efficient stabilization of state O^* relative to C_s^*.

On the basis of structural proximity of the NUDT9-H domain to the C-terminal end of the sixth TM α-helix (TM6), the nucleotide-activated slow gate is likely the TM6 bundle crossing that forms an intracellular gate in other members of the voltage-gated channel family [(6, 7); Fig. 6*G*, lower gate]; in other channels, this gate is regulated by intracellular agonists such as Ca^{2+} (24), phospholipids (25), or intracellular nucleotides (26). In contrast, the nucleotide-independent fast gate underlying the brief flickery closures might be formed by the extracellular selectivity filter (Fig. 6*G*, upper gate), which causes C-type inactivation of voltage-gated K^+ channels (27) and rundown of WT TRPM2 (11).

The scheme in Fig. 5*E* is a minimal scheme that accounts for many of our observations, but it allows for nucleotide binding/unbinding only in the closed state. However, deactivation time constants after nucleotide removal (Fig. 4) were consistently shorter than steady-state τ_b in saturating nucleotide (Fig. 6*B*), and a modest but significant trend for shortened steady-state τ_b was

observed at lower, submicromolar concentrations of ADPR (Fig. 6*B*, blue symbols). Because the rates of activation are very slow at these low ligand concentrations ($\tau_{ib} >> \tau_b$; cf. Fig. 6 *B* and *C*), macroscopic relaxation time constants on sudden lowering of ADPR concentration from saturating (32 μM) to 0.1 or 0.32 μM roughly measure the rates of deactivation at such submicromolar ADPR. Such relaxation time constants (τ_{relax}; Fig. S5*A*) were identical to τ_b measured at steady-state in 0.1 or 0.32 μM ADPR (Fig. S5*C*, open versus closed symbols), confirming that τ_{relax} on complete nucleotide removal (Fig. 4) indeed measures τ_b at zero ligand concentration. Although activation by ADPR necessarily implies that the nucleotide must be bound more tightly in the bursting state, this detectable ADPR concentration dependence of τ_b suggests incomplete occlusion of the ligand, with slow exchangeability even in the bursting state (i.e., the likely existence of unliganded states O and C_f, shown as semitransparent states in Fig. 6*G*). In contrast, coactivating Ca^{2+} ions were shown to remain at rapid equilibrium with the bulk cytosolic solution, even while a TRPM2 channel is open (10).

In conclusion, we have shown that TRPM2 is a conventional ligand-gated channel activated by ligand binding, and none of the observable gating transitions is coupled to the irreversible ADPR hydrolysis cycle reportedly catalyzed by its NUDT9-H domain. A practical consequence of this mechanism is that it outlines an obligate strategy for the design of specific TRPM2 modulators acting on the NUDT9-H domain: Activators should stabilize the bursting state by binding more tightly to bursting channels, whereas inhibitors should do the opposite (i.e., bind more tightly to closed channels). Further studies will need to verify enzymatic activity of the NUDT9-H domain, in isolation and in intact TRPM2 channels, as well as determine its physiologic relevance.

Materials and Methods

Molecular Biology. Mutations were introduced into TRPM2-pGEMHE (10) using Stratagene Quikchange. Linearized (NheI; New England BioLabs) cDNA was transcribed in vitro using T7 polymerase; cRNA was stored at −80 °C.

Isolation and Injection of *Xenopus* Oocytes. *Xenopus* oocytes were collagenase-digested, injected with 0.1–10 ng cRNA (for single-channel and macroscopic recordings, respectively), and stored at 18 °C. Recordings were done 1–3 d after injection.

Excised Inside-Out Patch-Clamp Recording. Pipette solution contained (in mM) 140 Na-gluconate, 2 Mg-gluconate$_2$, 10 Hepes (at pH 7.4 with NaOH; free $[Ca^{2+}]$ ~4 μM; the pipette electrode was placed into a 140-mM NaCl-based solution carefully layered on top] (10). Bath solution contained (in mM) 140 Na-gluconate, 2 Mg-gluconate$_2$, 10 Hepes (at pH 7.1 with NaOH), and either 1 mM EGTA [to obtain "zero" (~8 nM) Ca^{2+}] or 1 mM Ca-gluconate$_2$ (to obtain 125 μM free $[Ca^{2+}]$). Inward currents were recorded at 25 °C at a membrane potential of −20 mV; the cytosolic face of the patch was continuously superfused (solution exchange time constant, <50 ms). Currents were digitized at 10 kHz, filtered at 2 kHz, and recorded to disk. Na_2-ADPR was obtained from Sigma, and Na-AMPCPR was synthesized by Krzysztof Felczak (University of Minnesota), as described (18).

Data Analysis. Macroscopic current relaxations were least-squares fitted by single exponentials, and time constants after removal of AMPCPR were normalized to those of bracketing control relaxations on removal of 32 μM ADPR (Fig. S3*A*); averaged normalized time constants were rescaled by the pooled average for all control relaxations. Fractional currents (Figs. 1*G* and 3*C*) were calculated by dividing mean current in a test segment by mean current in 32 μM ADPR in the same patch. For steady-state single-channel kinetic analysis (Figs. 5 and 6), well-resolved current segments from single-channel (Fig. 5 *A* and *B*) or multichannel (Fig. S4 *A* and *C*) recordings were Gaussian-filtered at 200 Hz and idealized by the half-amplitude threshold method. The COC model was fitted to the events lists by maximum likelihood (ref. 28; Fig. S4 *B* and *D*), and τ_o, τ_b, τ_{ib}, τ_f, and n_f (Fig. 6) were calculated from the fitted rate constants, as described (19).

ACKNOWLEDGMENTS. This work was supported by an International Early Career Scientist grant from the Howard Hughes Medical Institute (to L.C.) and MTA Lendület Grant LP2012-39/2012.

1. Yamamoto S, et al. (2008) TRPM2-mediated Ca2+influx induces chemokine production in monocytes that aggravates inflammatory neutrophil infiltration. *Nat Med* 14(7):738–747.
2. Uchida K, et al. (2011) Lack of TRPM2 impaired insulin secretion and glucose metabolisms in mice. *Diabetes* 60(1):119–126.
3. Nilius B, Owsianik G, Voets T, Peters JA (2007) Transient receptor potential cation channels in disease. *Physiol Rev* 87(1):165–217.
4. Hermosura MC, et al. (2008) Altered functional properties of a TRPM2 variant in Guamanian ALS and PD. *Proc Natl Acad Sci USA* 105(46):18029–18034.
5. McQuillin A, et al. (2006) Fine mapping of a susceptibility locus for bipolar and genetically related unipolar affective disorders, to a region containing the C21ORF29 and TRPM2 genes on chromosome 21q22.3. *Mol Psychiatry* 11(2): 134–142.
6. Long SB, Campbell EB, Mackinnon R (2005) Crystal structure of a mammalian voltage-dependent Shaker family K+ channel. *Science* 309(5736):897–903.
7. Liao M, Cao E, Julius D, Cheng Y (2013) Structure of the TRPV1 ion channel determined by electron cryo-microscopy. *Nature* 504(7478):107–112.
8. Perraud AL, et al. (2001) ADP-ribose gating of the calcium-permeable LTRPC2 channel revealed by Nudix motif homology. *Nature* 411(6837):595–599.
9. Perraud AL, et al. (2005) Accumulation of free ADP-ribose from mitochondria mediates oxidative stress-induced gating of TRPM2 cation channels. *J Biol Chem* 280(7): 6138–6148.
10. Csanády L, Törocsik B (2009) Four Ca2+ ions activate TRPM2 channels by binding in deep crevices near the pore but intracellularly of the gate. *J Gen Physiol* 133(2): 189–203.
11. Tóth B, Csanády L (2012) Pore collapse underlies irreversible inactivation of TRPM2 cation channel currents. *Proc Natl Acad Sci USA* 109(33):13440–13445.
12. Perraud AL, et al. (2003) NUDT9, a member of the Nudix hydrolase family, is an evolutionarily conserved mitochondrial ADP-ribose pyrophosphatase. *J Biol Chem* 278(3):1794–1801.
13. Ramjeesingh M, et al. (1999) Walker mutations reveal loose relationship between catalytic and channel-gating activities of purified CFTR (cystic fibrosis transmembrane conductance regulator). *Biochemistry* 38(5):1463–1468.
14. Csanády L, Vergani P, Gadsby DC (2010) Strict coupling between CFTR's catalytic cycle and gating of its Cl- ion pore revealed by distributions of open channel burst durations. *Proc Natl Acad Sci USA* 107(3):1241–1246.
15. Csanády L, Töröcsik B (2014) Catalyst-like modulation of transition states for CFTR channel opening and closing: New stimulation strategy exploits nonequilibrium gating. *J Gen Physiol* 143(2):269–287.
16. Tóth B, Csanády L (2010) Identification of direct and indirect effectors of the transient receptor potential melastatin 2 (TRPM2) cation channel. *J Biol Chem* 285(39):30091–30102.
17. Shen BW, Perraud AL, Scharenberg A, Stoddard BL (2003) The crystal structure and mutational analysis of human NUDT9. *J Mol Biol* 332(2):385–398.
18. Pankiewicz KW, Lesiak K, Watanabe KA (1997) Efficient synthesis of methylenebis (phosphonate) analogues of P-1,P-2-disubstituted pyrophosphates of biological interest. A novel plausible mechanism. *J Am Chem Soc* 119:3691–3695.
19. Vergani P, Nairn AC, Gadsby DC (2003) On the mechanism of MgATP-dependent gating of CFTR Cl- channels. *J Gen Physiol* 121(1):17–36.
20. Runnels LW, Yue L, Clapham DE (2001) TRP-PLIK, a bifunctional protein with kinase and ion channel activities. *Science* 291(5506):1043–1047.
21. Kühn FJ, Lückhoff A (2004) Sites of the NUDT9-H domain critical for ADP-ribose activation of the cation channel TRPM2. *J Biol Chem* 279(45):46431–46437.
22. Colquhoun D, Sigworth FJ (1995) Part III. *Single-Channel Recording*, eds Sakmann B and Neher E (Plenum Press, New York).
23. Chakrapani S, Bailey TD, Auerbach A (2004) Gating dynamics of the acetylcholine receptor extracellular domain. *J Gen Physiol* 123(4):341–356.
24. Jiang Y, et al. (2002) Crystal structure and mechanism of a calcium-gated potassium channel. *Nature* 417(6888):515–522.
25. Hansen SB, Tao X, MacKinnon R (2011) Structural basis of PIP2 activation of the classical inward rectifier K+ channel Kir2.2. *Nature* 477(7365):495–498.
26. Zagotta WN, et al. (2003) Structural basis for modulation and agonist specificity of HCN pacemaker channels. *Nature* 425(6954):200–205.
27. Baukrowitz T, Yellen G (1995) Modulation of K+ current by frequency and external [K+]: A tale of two inactivation mechanisms. *Neuron* 15(4):951–960.
28. Csanády L (2000) Rapid kinetic analysis of multichannel records by a simultaneous fit to all dwell-time histograms. *Biophys J* 78(2):785–799.
29. Csanády L (2006) Statistical evaluation of ion-channel gating models based on distributions of log-likelihood ratios. *Biophys J* 90(10):3523–3545.